seems likely that these sampling differences account for the observed difference in the strength of correlations revealed by the two measures.

Received 26 June; accepted 19 November 1996.

1. Abeles, M. *Corticonics* (Cambridge Univ. Press, 1991).
2. Singer, W. & Gray, C. M. *Annu. Rev. Neurosci.* **18,** 555–586 (1995).
3. Engel, A. K., König, P., Kreiter, A. K., Schillen, T. B. & Singer, W. *Trends Neurosci.* **15,** 218–226 (1992).
4. Gray, C. M., König, P., Engel, A. K. & Singer, W. *Nature* **338,** 334–337 (1989).
5. Eckhorn, R. *et al. Biol. Cybern.* **60,** 121–130 (1988).
6. Bouyer, J. J., Montaron, M. F. & Rougeul, A. *Electroencephalogr. Clin. Neurophysiol.* **51,** 244–252 (1981).
7. Murthy, V. N. & Fetz, E. E. *Proc. Natl Acad. Sci. USA* **89,** 5670–5674 (1992).
8. Sanes, J. N. & Donoghue, J. P. *Proc. Natl Acad. Sci. USA* **90,** 4470–4474 (1993).
9. Vaadia, E. *et al. Nature* **373,** 515–518 (1995).
10. Bressler, S. L., Coppola, R. & Nakamura, R. *Nature* **366,** 153–156 (1993).
11. Scannell, J. W., Blakemore, C. & Young, M. P. *J. Neurosci.* **15,** 1463–1483 (1993).
12. Felleman, D. J. & Van Essen, D. C. *Cereb. Cortex* **1,** 1–47 (1991).
13. Maunsell, J. H. R. & Newsome, W. T. *Annu. Rev. Neurosci.* **10,** 363–401 (1987).
14. Goodale, M. A. & Milner, A. D. *Trends Neurosci.* **15,** 20–25 (1992).
15. Kalaska, J. F. & Crammond, D. J. *Science* **255,** 1517–1523 (1992).
16. Jeannerod, M., Arbib, M. A., Rizzolatti, G. & Sakata, H. *Trends Neurosci.* **18,** 314–320 (1995).
17. Mitzdorf, U. *Physiol. Rev.* **65,** 37–100 (1985).
18. Engel, A. K., Kreiter, A. K., König, P. & Singer, W. *Proc. Natl Acad. Sci. USA* **88,** 6048–6052 (1991).
19. Frien, A., Eckhorn, R., Bauer, R., Woelbern, T. & Kehr, H. *Neuroreport* **5,** 2273–2277 (1994).
20. Nelson, J. I., Salin, P. A., Munk, M. H. J., Arzi, M. & Bullier, J. *Vis. Neurosci.* **9,** 21–37 (1992).
21. Roelfsema, P. R., Engel, A. K., König, P. & Singer, W. *J. Cogn. Neurosci.* **8,** 603–625 (1996).
22. Engel, A. K., König, P., Kreiter, A. K. & Singer, W. *Science* **252,** 1177–1179 (1991).
23. Munk, M. H. J., Nowak, L. G., Nelson, J. I. & Bullier, J. *J. Neurophysiol.* **74,** 2401–2414 (1995).
24. Buchwald, N. A., Horvath, F. E., Wyers, E. J. & Wakefield, C. *Nature* **201,** 830–831 (1964).
25. Steriade, M., McCormick, D. A. & Sejnowski, T. J. *Science* **262,** 679–685 (1993).
26. Munk, M. H. J., Roelfsema, P. R., König, P., Engel, A. K. & Singer, W. *Science* **272,** 271–274 (1996).
27. Steriade, M., Amzica, F. & Contreras, D. *J. Neurosci.* **16,** 392–417 (1996).
28. Nieoullon, A. & Rispal-Padel, L. *Brain Res.* **105,** 405–422 (1976).
29. Tusa, R. J., Palmer, L. A. & Rosenquist, A. C. *J. Comp. Neurol.* **177,** 213–236 (1978).

ACKNOWLEDGEMENTS. We thank C. Stenner, N. Hensel and S. Herzog for technical assistance.

CORRESPONDENCE and requests for materials should be addressed to P.R.R. (e-mail: roelfsema@mpih-frankfurt.mpg.de).

In vivo dendritic calcium dynamics in neocortical pyramidal neurons

Karel Svoboda, Winfried Denk, David Kleinfeld* & David W. Tank

Biological Computation Research Department, Bell Laboratories, Lucent Technologies, Murray Hill, New Jersey 07974, USA

THE dendrites of mammalian pyramidal neurons contain a rich collection of active conductances that can support Na^+ and Ca^{2+} action potentials (for a review see ref. 1). The presence, site of initiation, and direction of propagation of Na^+ and Ca^{2+} action potentials are, however, controversial[2], and seem to be sensitive to resting membrane potential, ionic composition, and degree of channel inactivation, and depend on the intensity and pattern of synaptic stimulation. This makes it difficult to extrapolate from *in vitro* experiments to the situation in the intact brain. Here we show that two-photon excitation laser scanning microscopy[3] can penetrate the highly scattering tissue of the intact brain. We used this property to measure sensory stimulus-induced dendritic $[Ca^{2+}]$ dynamics of layer 2/3 pyramidal neurons of the rat primary vibrissa (Sm1) cortex *in vivo*. Simultaneous recordings of intracellular voltage and dendritic $[Ca^{2+}]$ dynamics during whisker stimulation or current injection showed increases in $[Ca^{2+}]$ only in coincidence with Na^+ action potentials. The amplitude of these $[Ca^{2+}]$ transients at a given location was approximately proportional to the number of Na^+ action potentials in a short burst. The amplitude for a given number of action potentials was greatest in the proximal apical dendrite and declined steeply with increasing distance from the soma, with little Ca^{2+} accumulation in the most distal branches, in layer 1. This suggests that widespread Ca^{2+} action potentials were not generated, and any significant $[Ca^{2+}]$ increase depends on somatically triggered Na^+ action potentials.

Although *in vivo* experiments provided some of the first evidence for active currents in dendrites[1], most of our understanding of the presence and role of these dendritic currents comes from *in vitro* brain-slice experiments using electrophysiological recording and optical imaging of $[Ca^{2+}]$. Such experiments have provided increasing evidence that Na^+ action potentials can, under appropriate conditions, propagate centrifugally into the dendritic tree of cortical pyramidal neurons[4]. Because these action potentials open voltage-dependent Ca^{2+} channels[5–8] and modulate voltage-dependent synaptic currents[9], they could be important in the control of long-term synaptic plasticity. Brain-slice experiments have also demonstrated Ca^{2+} action potentials in pyramidal cell dendrites[10,11] associated with very large dendritic Ca^{2+} accumulations[6,12]. However, dendritic excitability is strongly affected by a variety of biophysical parameters, such as ionic composition[13]. Furthermore, the site of dendritic action-potential initiation depends on the strength of synaptic excitation[8,14], and the activation of voltage-dependent conductances can be modulated by inhibitory synaptic inputs[15–17]. This implies that it is difficult to extrapolate from *in vitro* experiments to the intact nervous system. Thus understanding the presence and biological function of active dendritic currents requires measurements of membrane voltages[18] and dendritic ion dynamics in the intact nervous system in response to behaviourally relevant stimuli.

We measured $[Ca^{2+}]$ dynamics in neocortical neurons of anaesthetized rats by using a two-photon laser scanning microscope (TPLSM)[3] that allows imaging while the membrane potential is recorded using a microelectrode (Fig. 1*a*). In our TPLSM, two infrared photons produced by a mode-locked pulsed laser are simultaneously absorbed to excite fluorophores that normally absorb at visible wavelengths, with an absorption rate proportional to the square of the incident light intensity. Two-photon excitation was important for this experiment for several reasons[19]. First, infrared excitation provides greater depth penetration into the cortex than does visible light. Second, excitation is localized to the focal region (excitation volume $\sim 1\,\mu m^3$), providing three-dimensional optical sectioning and resolution equivalent to that of a confocal microscope without any loss of fluorescence light due to a detector pinhole, resulting in much reduced phototoxicity and photobleaching. Regular spiking[20] pyramidal cells in layer 2/3 of the primary vibrissa cortex (Sm1) were penetrated with sharp microelectrodes, and were iontophoretically filled with calcium green-1 (Fig. 1*b*). Dendrites were clearly resolved down to 500 μm below the pial surface, and three-dimensional cell morphology and location of electrode penetration could be reconstructed from stacks of images acquired at different depths (Fig. 1*c*). For $[Ca^{2+}]$ measurements at selected locations with high temporal resolution, line-scan mode was used[9].

Trains of whisker deflections (5 Hz, 2 s) produced a sequence of electrical events consisting of slow depolarizations, during which one, two or no Na^+ action potentials occurred (Fig. 1*d–f*). All slow depolarizations with Na^+ action potentials were quite large with low amplitude variability (Fig. 1*e*, *f*), whereas most that did not contain Na^+ action potentials were smaller and more variable in amplitude. The largest slow depolarizations ranged from 10 mV when recorded in the soma, to 40 mV when recorded in dendrites. Although they resembled large excitatory postsynaptic potentials[21], the uniformity of slow depolarizations associated with Na^+ action potentials also suggests that regenerative voltage-dependent conductances are involved. Simultaneous microelectrode measurements of membrane potential and fluorescence measurements of calcium indicator-filled dendrites ($n = 49$) revealed $[Ca^{2+}]$ transients that occurred in one-to-one correspondence with Na^+ action-potential bursts, with more action potentials leading to larger $[Ca^{2+}]$ transients (Fig. 1*d–f*, arrows). The transients had fast rise times (~2 ms) and short decay-time constants (< 100 ms).

* Present address: Department of Physics 0319, University of California, La Jolla, California 92093, USA.

To examine the possibility that Ca^{2+} current-mediated regenerative events are responsible for the uniformity of slow depolarizations, we examined more closely the $[Ca^{2+}]$ transient timecourse and the dependence of the $[Ca^{2+}]$ transient size on the number of action potentials contained in bursts produced by whisker stimulation and depolarizing current pulses. In the proximal dendrites, most of the $[Ca^{2+}]$ rise occurred within about 2 ms (the instrumental time resolution), and was coincident with the time of the Na^+ action potential, instead of rising gradually throughout the course of the underlying slow event (Fig. 2*a–f*), as would be expected for a Ca^{2+} action potential[6,12]. The size of the $[Ca^{2+}]$ transient closely followed the number of spikes in a burst (Fig. 2*g–i*), which is similar to observations in CA1 cells *in vitro*[22]. No significant influx occurred during large-amplitude slow depolarizations without Na^+ action potentials (Fig. 2*a*) or subthreshold depolarizing current pulses (Fig. 2*d*). Injection of hyperpolarizing current during whisker stimulation ($n = 5$) both increased the size of the slow depolarizations and also the fraction without Na^+ action potentials. Slow depolarizations without Na^+ action potentials, were still not accompanied by measurable $[Ca^{2+}]$ transients

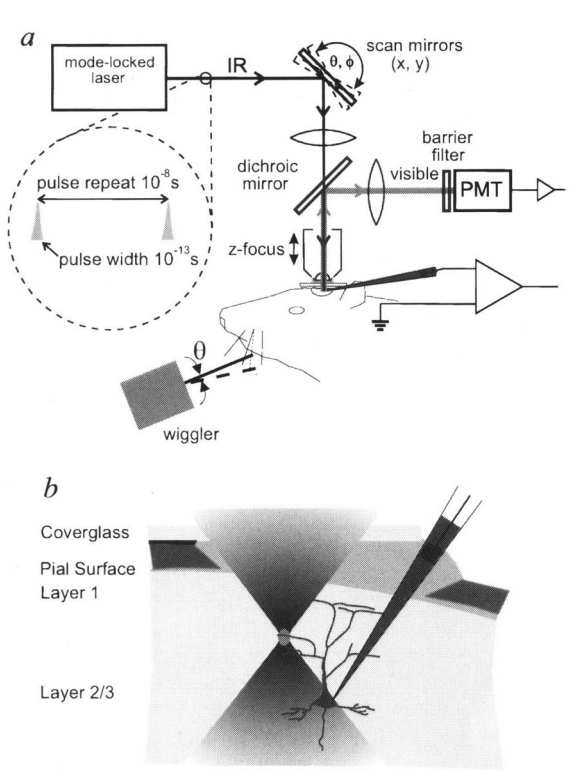

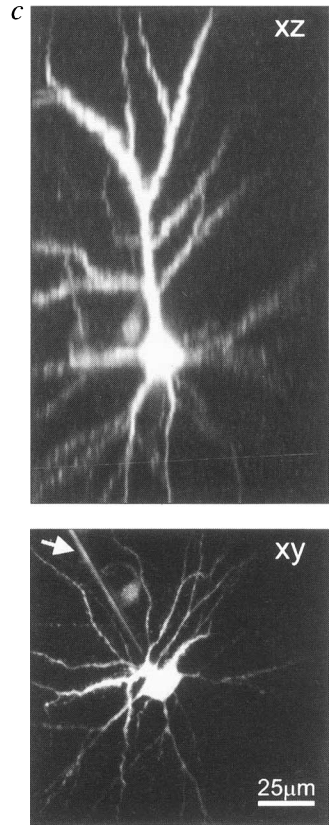

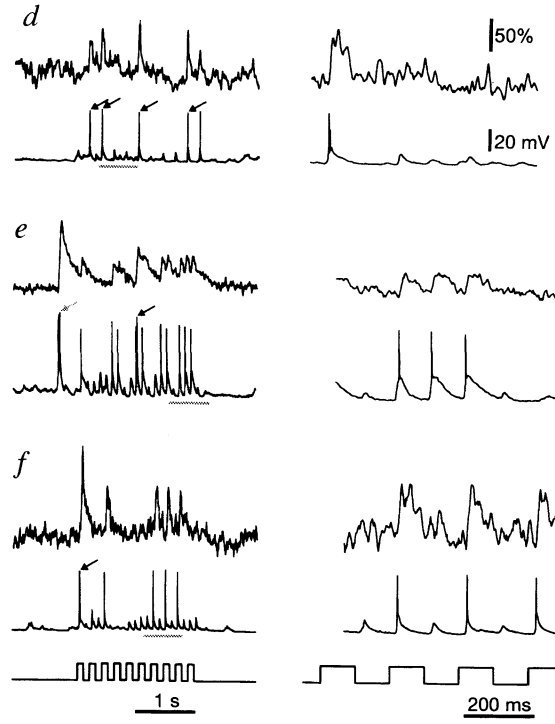

FIG. 1 *In vivo* two-photon excitation laser scanning microscopy (TPLSM) combined with sharp microelectrode recording in the primary vibrissa cortex of anaesthetized rats. *a*, Schematic representation of the experimental set-up, and *b*, representation of the recording and imaging geometry (neither to scale). *c*, Three-dimensional reconstruction of a layer 2/3 pyramidal neuron (projections onto the *x–z* (top) and *x–y* (bottom) planes; stack consists of 110 sections, 512 × 512 pixels each, acquired with 2-μm spacing). In the *x–z* projection the surface of the cortex is towards the top. *d–f*, Cellular responses to whisker stimulation for three representative cells. Left, recordings including one entire stimulus train; right, expanded views of sections indicated by grey bars. Action potentials (lower traces) were associated with dendritic $[Ca^{2+}]$ transients (upper traces), with two action potentials (black arrows) producing larger $[Ca^{2+}]$ transients. A spontaneous burst containing four action potentials (*e*, grey arrow), produced a still larger $[Ca^{2+}]$ transient. Whisker stimulus trains are shown at the bottom. Fluorescence was measured 150 μm above the soma and 290 μm below the pia (*d*), 60 μm above the soma and 170 μm below the pia (*e*), and 82 μm above the soma and 240 μm below the pia (*f*).

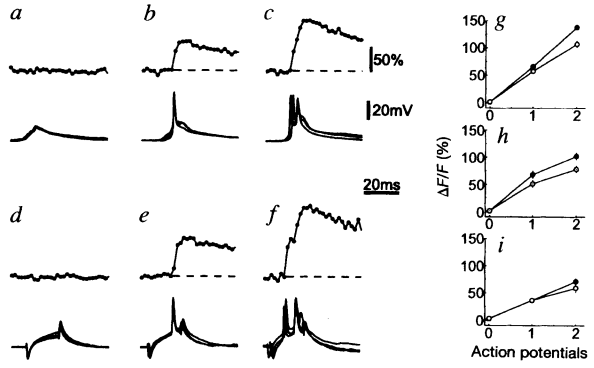

FIG. 2 Representative membrane-potential recordings (lower traces) and spike-triggered averages of $[Ca^{2+}]$ transient amplitude (upper traces; symbol spacing, 2 ms) *in vivo*. $[Ca^{2+}]$ transient and corresponding membrane potential in response to whisker stimulation (*a–c*) and current injection (*d–f*) evoking zero (*a*, $n = 49$; *d*, $n = 22$), one (*b*, $n = 76$; *e*, $n = 27$), or two (*c*, $n = 57$; *f*, $n = 28$) action potentials. In *c* and *f* averaging was triggered on the second action potential of the pair. *g–i*, Plots of peak $[Ca^{2+}]$ transient as a function of action-potential number (open circles, whisker stimulation; filled circles, current injection stimulation). *g*, Apical dendrite (82 μm above the soma, 240 μm below the pia. *h*, Apical dendrite (150 μm above the soma, 290 μm below the pia). *i*, Basal dendrite (20 μm below the soma, 180 μm below the pia).

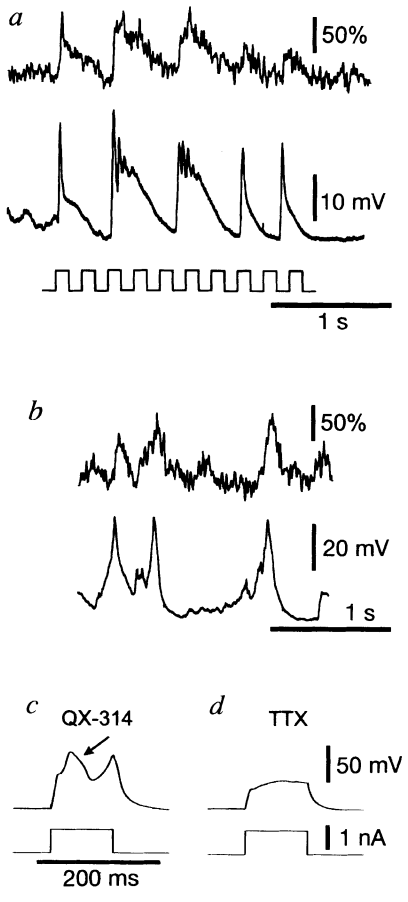

FIG. 3 Effects of QX-314 on electrogenesis *in vivo* (*a*, *b*) and *in vitro* (*c*, *d*). *a*, Dendritic $[Ca^{2+}]$ transient (top) and electrical response (middle) to whisker stimulation (bottom); fluorescence measured 50 μm above the soma and 210 μm below the pial surface. *b*, Spontaneous electrogenesis and associated $[Ca^{2+}]$ transient in a superficial neuron; fluorescence measured 50 μm above the soma and 100 μm below the pial surface. *c*, Membrane potential (upper trace) in response to a current pulse (lower trace) in a layer 2/3 pyramidal neuron measured *in vitro*, with intracellular QX-314. *d*, Response in another cell with tetrodotoxin (TTX) in the bath.

(data not shown). We conclude that uniformity of slow depolarizations is not produced by a widespread Ca^{2+} action potential, and that the $[Ca^{2+}]$ transients we observe are produced by the opening of voltage-dependent Ca^{2+} channels during Na^+ action potentials.

To further test whether Ca^{2+} action potentials were triggered by whisker deflection, we recorded from neurons in which Na^+ action potentials were abolished by QX-314 ($n = 6$). Dendritic $[Ca^{2+}]$ transients during whisker stimulation now tracked all of the slow depolarizing waveforms, some of which contained oscillations suggesting calcium electrogenesis (Fig. 3*a*). We also observed large spontaneous membrane-potential excursions (10–30 mV) accompanied by Ca^{2+} influx (Fig. 3*b*). Further, in neocortical brain slices, intracellular application of QX-314 to layer 2/3 pyramidal neurons produced Ca^{2+} action potentials in response to somatic current injections (Fig. 3*c*, arrow; $n = 4$), but extracellular application of tetrodotoxin, a highly specific Na^+-channel blocker, did not have this effect (Fig. 3*d*; $n = 4$). Together these results demonstrate that QX-314 assists the generation of Ca^{2+} action potentials *in vivo* (Fig. 3*a*) and *in vitro* (Fig. 3*c*), possibly by blocking K^+ channels[6,12,23,24]. More importantly, these results show that our imaging technique is sensitive enough to detect Ca^{2+} action potentials if they occur (Fig. 3*a*, *b*).

Although our data demonstrate that the uniformity of slow depolarizations is not produced by a widespread Ca^{2+} action potential, we have not ruled out the possibility that it is due to localized Ca^{2+} action potentials in dendritic regions, such as the numerous basal dendrites, that were not sampled adequately in our experiments. However, in slice recordings, dendritic Ca^{2+} action potentials generate the largest and most distributed $[Ca^{2+}]$ transients[6], so we do not consider localized dendritic Ca^{2+} action potentials to be a likely explanation for our data. An alternative explanation for the uniformity of slow depolarizations is that they are produced by other regenerative currents, which might not cause Ca^{2+} influx, such as the low-voltage-gated Na^+ current responsible for membrane oscillations in cortical pyramidal cells[25]. An altogether different explanation may be the generation of uniform synaptic input as a result of some collective network excitation.

The $[Ca^{2+}]$ transient associated with a Na^+ action potential has been reported to be a uniform global signal in the dendrite[8]. It has also been reported to show a strong spatial dependence[26]. We examined this issue *in vivo* by mapping the spatial pattern of $[Ca^{2+}]$ transient amplitude in the apical dendrite (Fig. 4*a*) in response to whisker stimulation (Fig. 4*b*; $n = 3$), current injection (Fig. 4*c*; $n = 2$) and extracellular stimulation (Fig. 4*d*; $n = 1$). For all three stimuli, the $[Ca^{2+}]$ transient amplitude was largest in the proximal apical dendrite, peaking within ~100 μm of the soma. Beyond 100 μm the amplitude decreased with distance from the soma, with no detectable $[Ca^{2+}]$ rise in the tufted branches of layer 1 (Fig. 4*a–d*). The absence of $[Ca^{2+}]$ transients in layer 1 was confirmed in other cells ($n = 7$), without constructing a complete map. Under all stimulating conditions, somatic $[Ca^{2+}]$ transients were clearly present but were small, possibly owing to the unfavourable surface-to-volume ratio, in agreement with *in vitro* measurements[5,6]. The amplitudes of $[Ca^{2+}]$ transients in basal dendrites in the vicinity of the soma (<50 μm away) were similar to the largest values found for apical dendrites (Figs 2*i* and 4*b*). However, because basal dendrites are thin and deeply embedded in the tissue they were often not bright enough for us to map the $[Ca^{2+}]$ transient amplitude as a function of distance from the soma.

We have demonstrated that TPLSM can be used to measure $[Ca^{2+}]$ dynamics in the dendrites of neurons in the intact mammalian brain. Our measurements render it unlikely that the large-amplitude, low-variability slow depolarizations produced by sensory stimulation in the anaesthetized rat are Ca^{2+} action potentials. The amplitude and spatial pattern of $[Ca^{2+}]$ transients produced by sensory stimulation is dominated by the effects of Na^+ action-potential depolarization. The fall-off of the $[Ca^{2+}]$

transients with distance, which could be caused by Na^+ action-potential propagation failure or by a non-homogenous distribution of voltage-dependent Ca^{2+} channels[5,26], is even steeper than reported in CA1 hippocampal pyramidal cells *in vitro*[26], and distinctly different from the unattenuated global $[Ca^{2+}]$ signal that has also been reported in CA1 cells[8]. The spatial pattern we have observed might imply spatially varying mechanisms or conditions for the induction of Ca^{2+}-dependent long-term synaptic plasticity[27] in the highly stratified afferent inputs in neocortex. However, the largest $[Ca^{2+}]$ transients on the apical dendrite of layer 2/3 neurons occur in a region devoid of synaptic spines and also, presumably, of excitatory (glutamergic) input. Given the sensitivity of dendritic excitability on K^+ channel modulation[6,12,24], it will be interesting to examine whether the pattern we measured is altered by the neuromodulatory influence of cortical activating systems. Our failure to observe Ca^{2+} action potentials in regular spiking layer 2/3 cells does not rule out the presence of regenerative Ca^{2+} events under different stimulus conditions or during different behavioural states. Further experiments using TPLSM might help to address these issues. □

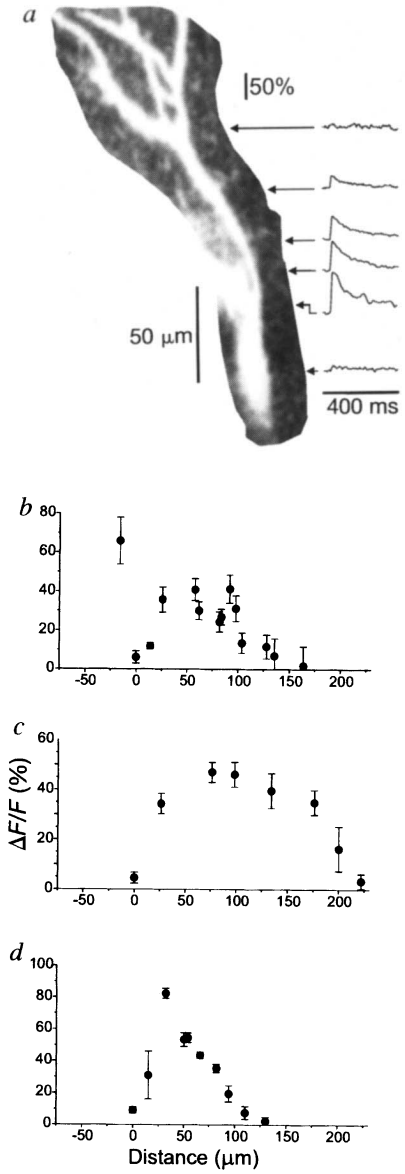

FIG. 4 Spatial maps of average $[Ca^{2+}]$ transient amplitude in apical dendrites of layer 2/3 neurons *in vivo* using different stimuli. *a*, Layer 2/3 neuron *in vivo* (projections onto the *x*–*z* plane; stack consists of 115 sections, 256 × 256 pixels each, 2 μm spacing; surface of the cortex is towards the top. Right, selected $[Ca^{2+}]$ transients (average of 5–10 responses). *b*, Whisker deflections (soma 260 μm below the pia). The averaging of $[Ca^{2+}]$ transients was triggered on extracellularly recorded spikes after electrode withdrawal. *c*, Current injection evoking two Na^+ action potentials (soma was 415 μm below the pia). The averaging of the fluorescence signal was triggered on the second Na^+ action potential. *d*, Extracellular stimulation (1 MΩ monopolar glass electrode filled with 1 M NaCl; 100 μs pulses) on the border of layers 1 and 2 (soma 280 μm below the pia). The averaging of the $[Ca^{2+}]$ transient was triggered on the stimulus artefact (same cell as in *a*).

Methods

***In vivo* imaging and electrophysiology.** Rats (4–6 weeks, $n = 50$) were anaesthetized with urethane (2 mg per g body weight, administered intraperitoneally), a small craniotomy (3 × 3 mm) was cut above primary vibrissa cortex, and the dura was removed. The exposed area was covered with 2% agarose (Type III-A, Sigma, in artificial cerebrospinal fluid) and a coverslide mounted on a stainless-steel frame[28] that was secured to the skull with dental cement and fixed to the microscope stage. Sharp electrodes were filled with 400 mM K-acetate and 3 mM calcium green-1 (Molecular Probes) and bevelled (resistance ~50–100 MΩ). In some cases electrodes also contained 30 mM Lidocaine *N*-ethyl bromide (QX-314, Research Biochemicals International). Membrane-potential recordings were made with an intracellular amplifier (Neurodata IR283) and stored digitally. Neurons with resting potentials more negative than −55 mV were iontophoretically filled with indicator dye by injecting them with hyperpolarizing current (−0.2 to −0.5 nA, 5 to 15 min). During filling, a thin pencil lead attached to a galvanometer scanner was used to deflect one to three whiskers by 5–20 deg in a sequence of ten square deflections at 5 Hz, similar to whisker movement frequencies and amplitudes during tactile discrimination[29]. Simultaneously, stimulator position was adjusted until a cellular response was detected. No attempt was made to identify the principal whisker. After filling, the electrode was either withdrawn ($n = 18$) or the hyperpolarizing current was turned off ($n = 49$). Cell input resistances ranged from 20 to 120 MΩ, and action-potential amplitudes from 40 to 85 mV. Intracellular recordings lasted between 20 min and 2 h. Electrical recordings with and without ($n = 4$) Ca^{2+} indicator in the electrode were indistinguishable. Imaging was performed with a custom-made laser scanning microscope. The light source for two-photon excitation was a pulsed Ti:sapphire laser (Tsunami; Spectra Physics) operating at 80 MHz repeat frequency, 100 fs pulse width, and wavelength of between 800 and 850 nm. Excitation light was focused by a ×40 water-immersion objective lens (0.75 NA; Carl Zeiss). The average power delivered to the brain was <200 mW. Scanning was performed using two galvanometer mirrors (Cambridge Technology, model 6800). Scanning and image acquisition were controlled with custom software. Emitted light was collected in epifluorescence mode and detected with a photomultiplier tube (Hamamatsu R9638). Acquisition of images and electrophysiology was synchronized to 125 μs. Fast fluorescence measurements were achieved by repeatedly scanning a single line across the dendrite at 2-ms time intervals. The resulting line-scan image was used for quantitative analysis as follows: the fluorescence signal, F, was computed as an average along the scan line over the width of the dendrite or soma; the baseline signal, F_{base}, was computed as an average over the same width for several scan lines before an event; the normalized change in fluorescence was then $\Delta F/F = (F - F_{base})/(F_{base} - B)$, where B is the background signal determined from averages on areas adjacent to the dendrite. Apart from dye saturation, $\Delta F/F$ is proportional to $\Delta[Ca^{2+}]$. Action potential-evoked $[Ca^{2+}]$ transients had short decay time constants (<100 ms) (ref. 22). For current injection experiments, current pulses (20 ms) were injected into neurons at 2 Hz. The current amplitude was adjusted to stochastically generate zero, one or two Na^+ action potentials. For both whisker stimulation and current injection stimulation, events with zero, one or two action potentials were grouped, respectively, and spike triggered averages of $\Delta F/F$ were computed. To quantify the size of the $[Ca^{2+}]$ transients, the peak response was computed as an average over three scan lines around the peak of the response; because of motion-related fluctuations of the fluorescence signal at heartbeat (~7 Hz) and breathing frequencies (~2 Hz), this measure was found to be more reliable than the integral of the response. The dependence of $\Delta[Ca^{2+}]$ on action-potential number occasionally contained a slight compressive nonlinearity (see Fig. 2*h*). Considering that the dendritic $[Ca^{2+}]$ rise in response to a single Na^+ action potential can approach the K_d of the indicator[22], dye saturation may be responsible[30], but Na^+ spike waveform changes and Ca^{2+}-channel inactivation may also contribute. Considering that synaptic activation produces localized Ca^{2+} influx *in vitro*[9], our failure to detect calcium transients in response to subthreshold slow depolarization (Fig. 2*a*) may seem surprising. But a slow depolarization might be the result of activation of tens of synapses, less than 1% of the total, and our technique samples on the order of 1 μm of dendrite at any time. It would therefore be very difficult to find Ca^{2+} transients associated with synaptic activation at an unknown location in the dendritic tree[9]. In some mapping experiments during which the electrode was not withdrawn (Fig. 4*c*), indicator gradients might have reduced $\Delta F/F$ close to the site of the electrode penetration, where the dye concentration is highest. Our

basic conclusion, that $[Ca^{2+}]$ transients peak close to the soma with little influx in the distal braches of layer 1, would thus not be affected. In some cases (Fig. 4*b*, *d*), to dissipate dye gradients, Ca^{2+} transient were recorded more than 30 min after electrode withdrawal. All data are presented as mean ± s.e.m.

Brain-slice preparation, imaging and electrophysiology. Rats (4–6 weeks old) were deeply anaesthetized (50 mg ml^{-1} Nembutal) and decapitated. The brain was removed and coronal slices (300 μm thick) from somatosensory cortex were cut with a vibratome. Slices were kept at 33 °C for 30min and subsequently stored at room temperature (22–24 °C). After 1–5 h slices were transferred to a submerged recording chamber (22–24 °C). The artificial cerebrospinal fluid contained (in mM): 124 NaCl, 26 $NaHCO_3$, 3 KCl, 1.25 NaH_2PO4, 2 $MgSO_4$, 10 dextrose, 2 $CaCl_2$, saturated with 95% O_2/5% CO_2 (pH 7.3; osmolarity, 290–300 mOsm). In some cases 1 μM of tetrodotoxin was added. Whole-cell recordings were established under visual control, and recordings were made with a patch-clamp amplifier (EPC-7; List Electronics) operating in current-clamp mode. Resistance compensation was performed off-line. Electrodes had resistances of 7–10 MΩ when filled with internal solution containing (in mM): 135 K-methanesulphonate (Fluka), 10 K-HEPES, 2 $MgCl_2$, 3 Na_2ATP, 0.2 EGTA and 0.1 calcium green-1 (Molecular Probes) (pH, 7.2–7.3; osmolarity, 280 mOsm). In some experiments 6 mM QX-314 was added. Access resistances after break-in were 15–30 MΩ. Measurements were started 20 min after break-in.

Received 5 August; accepted 14 November 1996.

1. Yuste, R. & Tank, D. W. *Neuron* **16,** 701–716 (1996).
2. Regehr, W. G. & Armstrong, C. M. *Curr. Biol.* **4,** 436–439 (1994).
3. Denk, W., Strickler, J. H. & Webb, W. W. *Science* **248,** 73–76 (1990).
4. Stuart, G. J. & Sakmann, B. *Nature* **367,** 69–72 (1994).
5. Regehr, W. G., Connor, J. A. & Tank, D. W. *Nature* **341,** 533–536 (1989).
6. Jaffe, D. B. *et al. Nature* **357,** 244–246 (1992).
7. Magee, J. C. & Johnston, D. *Science* **268,** 301–304 (1995).
8. Spruston, N., Schiller, Y., Stuart, G. & Sakmann, B. *Science* **268,** 297–300 (1995).
9. Yuste, R. & Denk, W. *Nature* **375,** 682–684 (1995).
10. Wong, R. K. S., Prince, D. A. & Basbaum, A. I. *Proc. Natl Acad. Sci. USA* **76,** 986–990 (1979).
11. Kim, H. G. & Connors, B. W. *J. Neurosci.* **13,** 5301–5311 (1993).
12. Yuste, R., Gutnick, M. J., Saar, D., Delaney, K. R. & Tank, D. W. *Neuron* **13,** 23–43 (1994).
13. Andreasen, M. & Lambert, J. D. C. *J. Physiol. (Lond.)* **483,** 421–441 (1995).
14. Turner, R. W., Meyers, E. R., Richardson, D. L. & Barker, J. L. *J. Neurosci.* **11,** 2270–2280 (1991).
15. Kim, H. G., Beierlein, M. & Connors, B. W. *J. Neurophysiol.* **74,** 1810–1814 (1995).
16. Buzsaki, G., Penttonen, M., Nadasdy, Z. & Bragin, A. *Proc. Natl Acad. Sci. USA* **93,** 9921–9925 (1996).
17. Tsubokawa, H. & Ross, W. N. *J. Neurophysiol.* **76,** 2896–2906 (1996).
18. Hirsch, J. A., Alonso, J.-M. & Reid, R. C. *Nature* **378,** 612–616 (1995).
19. Denk, W. *et al. J. Neurosci. Methods* **54,** 151–162 (1994).
20. Connors, B. W. & Gutnick, M. J. *Trends Neurosci.* **13,** 99–104 (1990).
21. Carvell, G. E. & Simons, D. J. *Brain Res.* **448,** 186–191 (1988).
22. Helmchen, F., Imoto, K. & Sakmann, B. *Biophys. J.* **70,** 1069–1081 (1996).
23. Andreasen, M. & Hablitz, J. J. *J. Neurophysiol.* **69,** 1966–1975 (1993).
24. Reuveni, I., Friedman, A., Amitai, Y. & Gutnick, M. J. *J. Neurosci.* **13,** 4609–4621 (1993).
25. Gutfreund, Y., Yarom, Y. & Segev, I. *J. Physiol. (Lond.)* **483,** 621–640 (1995).
26. Callaway, J. C. & Ross, W. N. *J. Neurophysiol.* **74,** 1395–1403 (1995).
27. Bear, M. F. & Malenka, R. C. *Curr. Opin. Neurobiol.* **4,** 389–399 (1994).
28. Kleinfeld, D. & Delaney, K. R. *J. Comp. Neurol.* **375,** 89–108 (1996).
29. Carvell, G. E. & Simons, D. J. *J. Neurosci.* **10,** 2638–2648 (1990).
30. Feller, ,M. B., Delaney, K. R. & Tank, D. W. *J. Neurophysiol.* **76,** 381–401 (1996).

ACKNOWLEDGEMENTS. We thank R. Stepnoski for writing the software controlling the microscope, and G. Buzsaki, M. Fee and Z. Mainen for discussion.

CORRESPONDENCE and requests for materials should be addressed to W.D. (e-mail: denk@bell-labs.com) or D.W.T. (e-mail: dwt@physics.lucent.com).

Role of melanocortinergic neurons in feeding and the *agouti* obesity syndrome

Wei Fan*, Bruce A. Boston*†, Robert A. Kesterson*, Victor J. Hruby‡ & Roger D. Cone*

* The Vollum Institute for Advanced Biomedical Research, and
† Department of Pediatrics, Oregon Health Sciences University,
3181 S. W. Sam Jackson Park Road, Portland, Oregon 97201, USA
‡ Department of Chemistry, University of Arizona, Tucson, Arizona 85721, USA

DOMINANT alleles at the *agouti* locus (*A*) cause an obesity syndrome in the mouse, as a consequence of ectopic expression of the *agouti* peptide[1–6]. This peptide, normally only found in the skin, is a high-affinity antagonist of the melanocyte-stimulating hormone receptor (MC1-R)[7], thus explaining the inhibitory effect of *agouti* on eumelanin pigment synthesis. The *agouti* peptide is also an antagonist of the hypothalamic melanocortin-4 receptor (MC4-R)[7–9]. To test the hypothesis that *agouti* causes obesity by antagonism of hypothalamic melanocortin receptors[7], we identified cyclic melanocortin analogues[10] that are potent agonists or antagonists of the neural MC3 (refs 11, 12) and MC4 receptors. Intracerebroventricular administration of the agonist, MTII, inhibited feeding in four models of hyperphagia: fasted C57BL/6J, *ob/ob*, and A^Y mice, and mice injected with neuropeptide Y. Co-administration of the specific melanocortin antagonist and *agouti*-mimetic SHU9119 completely blocked this inhibition. Furthermore, administration of SHU9119 significantly enhanced nocturnal feeding, or feeding stimulated by a prior fast. Our data show that melanocortinergic neurons exert a tonic inhibition of feeding behaviour. Chronic disruption of this inhibitory signal is a likely explanation of the *agouti* obesity syndrome.

The *agouti* peptide acts as a paracrine factor in the regulation of eumelanin (brown–black pigment) synthesis, and in the induction of obesity[13]. The non-endocrine nature of the peptide and the lack of homogeneous preparations have complicated analysis of the activities of the peptide *in vivo*. Screening analogues of the cyclic lactam melanocortin agonist MTII (Ac-Nle^4-c[Asp^5, D-Phe^7, Lys^{10}]α-MSH-(4-10)-NH_2) led to the identification of the *agouti*-mimetic SHU9119 (Ac-Nle^4-c[Asp^5, D-2′Nal^7, Lys^{10}]α-MSH-4-10)-NH_2)[10] (Fig. 1*a*). This compound shares pharmacological properties with *agouti* peptide in that it is a potent antagonist of MC4-R and a less potent antagonist of the MC3-R[7] (Fig. 1*b*). The closely related analogue MTII (ref. 14) is identical to SHU9119 with the exception of a D-phenylalanine in place of the D-2′naphthylalanine, and is a full agonist of the MC3-R and MC4-R (Fig. 1*b*).

Mice were induced to feed by food deprivation for 16 h before intracerebroventricular (ICV) administration of the nonspecific melanocortin agonist MTII. In comparison to vehicle-injected animals, MTII was found to produce a potent inhibition of feeding within one hour of administration (Fig. 2*a*). At the highest dose (3 nmol), food intake was significantly inhibited for up to 4 h after administration ($P < 0.001$), and decreased food intake continued for the next 4 h, with normal rates resuming about 8 h after treatment. There was a dose–response relationship between MTII dose and feeding inhibition, with an IC_{50} at the 2-h time point of 0.6 nmol. Inhibition of feeding with 3 nmol MTII was blocked by co-administration of 6 nmol SHU9119 (Fig. 2*b*; $P < 0.001$), demonstrating that the effect results specifically from agonist binding to MC4-R and/or MC3-R.

MTII-treated mice were alert and exhibited no unusual behaviour relative to controls. The effect of MTII on locomotor activity was tested by using sound- and light-proof cages containing multiple light-beam detectors. The movements of MTII- and vehicle-treated mice were measured during two 90-min time periods (0.5–2 h, Fig. 2*c*; 2.5–4 h, data not shown) after ICV administration. The higher initial activity, indicative of exploratory behaviour, and continued locomotion were indistinguishable between the two groups, indicating that the inhibition of feeding was not due to decreased arousal or locomotion. In contrast to its long-term inhibition of feeding (4–8 h), MTII only inhibited drinking in water-deprived animals during a brief time period (<1 h) after administration (Fig. 2*d*).

The administration of MTII also inhibited food intake in three other models of hyperphagia, involving C57BL/6J-*Lep*^{ob}, C57BL/6J-A^Y and neuropeptide Y (NPY)-injected C57BL/6J mice. The hyperphagia in these models can be seen clearly by comparing the 12 h food intake after a fast in vehicle-injected C57BL/6J (2.4 g; Fig. 2*a*), C57BL/6J-A^Y (3.7 g, Fig. 3*a*) and C57BL/6J-*Lep*^{ob} (3.7 g; Fig. 3*c*) animals. As expected, MTII treatment inhibited food intake after a 16-h fast in the C57BL/6J-A^Y mouse (Fig. 3*a*; $P < 0.05$).

MTII, when co-administered with NPY, significantly inhibited the profound stimulation of feeding normally induced by NPY,